RSC Advances

PAPER

View Article Online
View Journal | View Issue

Cite this: *RSC Adv.*, 2022, **12**, 33922

A water-soluble fluorescent probe for monitoring mitochondrial GSH fluctuations during oxidative stress†

Huayu Wang, ‡[a] Luan Zhang,‡[b] Xia Jin,[b] Peijiao Tian,[b] Xiaojun Ding[b] and Jing Chang*[b]

Received 29th July 2022
Accepted 7th October 2022

DOI: 10.1039/d2ra04732b

rsc.li/rsc-advances

In this research, we constructed a styrylpyridine derivative-based fluorescent probe **MITO-PQDNs** to monitor mitochondrial glutathione (GSH). The probe **MITO-PQDNs** could react rapidly (20 min) with GSH in PBS buffer and exhibited a strong fluorescence signal (586 nm) as well as a significant Stokes shift (200 nm). Moreover, **MITO-PQDNs** could quantitatively detect GSH with high sensitivity (LOD = 253 nM). Meanwhile, **MITO-PQDNs** possessed favorable biocompatibility and could detect both endogenous and exogenous GSH in MCF-7 cells. Above all, **MITO-PQDNs** enabled the detection of fluctuations in mitochondrial GSH concentrations during oxidative stress.

1. Introduction

As a critical organelle involved in aerobic respiration, mitochondria can consume oxygen and carbohydrates, thus releasing adenosine triphosphate (ATP), which provides the most energy for cellular activity.[1] Meanwhile, mitochondria play an essential role in signaling, cell differentiation, cell apoptosis, maintenance of calcium homeostasis, *etc.*[2–4] Mitochondria are the major site of production of reactive oxygen species (ROS), and excess ROS induces cells to be in a state of oxidative stress, ultimately leading to a range of diseases such as neurodegenerative diseases and cancer.[5,6] Mitochondrial glutathione (GSH, the most abundant biothiol in cells) can scavenge excess mitochondrial ROS generated during aerobic metabolism and thus control the damage caused by oxidative stress.[7,8] In addition, mitochondrial GSH also plays a major role in biological processes, for example regulating cell death.[9,10] Hence, it is of practical importance to achieve the visual monitoring of mitochondrial GSH.

Owing to the advantages of non-invasiveness, high sensitivity, favorable biocompatibility, and high spatiotemporal resolution, organic small molecule fluorescent probes have become a powerful tool for monitoring GSH *in vitro* and *vivo*.[11–13] Many researchers have focused on developing the GSH-specific fluorescent probes capable of targeting mitochondria, and some achievements have been made.[14–17] In 2018, Liu *et al.* developed a hemicyanine-based ratiometric fluorescent probe **1** that specifically recognized mitochondrial GSH through nucleophilic aromatic substitution reaction (SNAr) and aldimine condensation reaction.[18] In 2021, Zhu *et al.* constructed a mitochondrial-targeted fluorescent probe **QZ** based on rhodamine B derivative, and the presence of aromatic thioester bond of **QZ** ensured its high selectivity for GSH.[19] In 2022, Zhou *et al.* designed a near-infrared (NIR) fluorescent probe **JGP** based on the intramolecular charge transfer (ICT) mechanism to monitor mitochondrial GSH.[20] The probe **JGP** was composed of a cyanine fluorophore, an indole ammonium cation targeting group and a 2,4-dinitrobenzenesulfonyl recognition site, and triumphantly achieved the bioimaging of GSH in *Caenorhabditis elegans* and rat brain slices. However, these fluorescent probes, which possessed poor water-solubility, could usually only detect analytes in solutions containing organic cosolvents. Consequently, fluorescent probes must be further developed to detect mitochondrial GSH in a pure water system specifically.

In this work, we constructed a styrylpyridinium-based fluorescent probe **MITO-PQDNs** with superb water solubility (Scheme 1). By introducing a rigid piperazine ring into the *para*-position of the benzene ring, the strong intramolecular electron push–pull effect of the fluorophore **MITO-PQ** was achieved, resulting in a strong ICT effect and long emission wavelength.[21] The 2,4-dinitrophenylsulfonyl (DNs) group with strong electron-absorbing ability could significantly quench the fluorescence of the fluorophore **MITO-PQ** and react with the sulfhydryl group of GSH, so the DNs group was selected as the recognition moiety for **MITO-PQDNs**.[20,22] Furthermore, the pyridine salt moiety with a positive charge could bind tightly to the inner mitochondrial membrane with a negative potential of −180 mV, which allowed the probe **MITO-PQDNs** to be selectively

[a]*School of Basic Medical Sciences, Xinxiang Medical University, Xinxiang 453003, China*

[b]*Jiangsu Mai Jian Biotechnology Development Company, Wuxi 214135, China. E-mail: chang_jing09@aliyun.com*

† Electronic supplementary information (ESI) available. See DOI: https://doi.org/10.1039/d2ra04732b

‡ Huayu Wang and Luan Zhang contributed equally to this work.

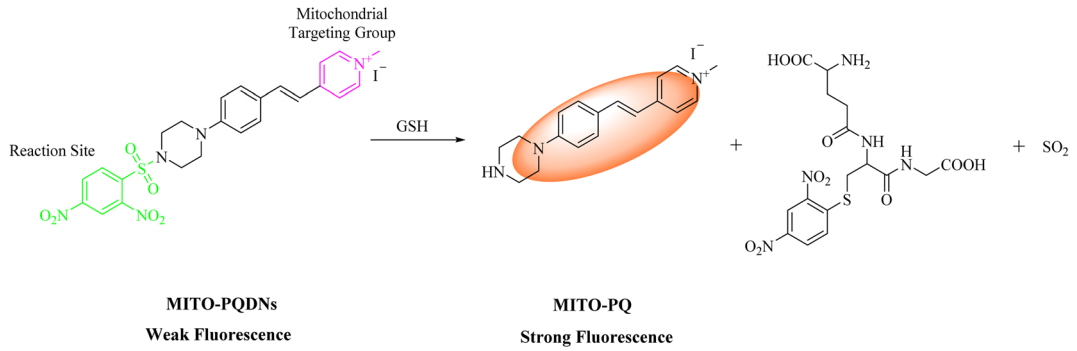

Scheme 1 The design strategy of MITO-PQDNs and the response mechanism of MITO-PQDNs with GSH.

enriched in mitochondria.[23–28] However, most of the available pyridinium probes had small Stokes shifts, resulting in strong self-absorption which would be detrimental to fluorescence imaging applications. In comparison, **MITO-PQDNs** could react rapidly with GSH in PBS buffer, thus showing intense yellow fluorescence (586 nm) as well as significant Stokes shift (200 nm). **MITO-PQDNs** exhibited excellent mitochondrial targeting ability and successfully monitored the dynamic changes in mitochondrial GSH levels during oxidative stress. Hence, **MITO-PQDNs** was expected to be a powerful chemical tool for monitoring mitochondrial GSH.

2. Materials and methods

2.1. Synthesis and characterization of the probe MITO-PQDNs

The fluorophore **MITO-PQ** was used as the initial material and was prepared according to the reported literature.[21] The synthesis method of the probe **MITO-PQDNs** was depicted in Scheme 2.

MITO-PQ (336.5 mg, 1.2 mmol) and triethylamine (700.0 μL, 5 mmol) were added sequentially into 25 mL of anhydrous dichloromethane (DCM) at 0 °C. After the solid was fully dissolved, 2,4-dinitrobenzenesulfonyl chloride (399.9 mg, 1.5 mmol) dissolved in 10 mL of DCM was slowly added to the mixture under stirring. The reaction was stopped when the mixture was stirred at 0 °C for 9 h. After removal of the solvent under reduced pressure, the probe **MITO-PQDNs** was purified by silica gel column chromatography (yield: 58.6%). ^{1}H NMR (400 MHz, DMSO-d_6) δ 9.01 (s, 1H), 8.75 (d, J = 6.8 Hz, 2H), 8.59(dd, J = 8.8, 2.4 Hz, 1H), 8.32 (d, J = 8.8 Hz, 1H), 8.05–8.11 (m, 2H), 7.89 (d, J = 16.4 Hz, 1H), 7.61 (d, J = 8.8 Hz, 2H), 7.27 (d, J = 8.8 Hz, 1H), 7.04 (d, J = 8.8 Hz, 2H), 4.21 (s, 3H), 3.40–3.46 (m, 4H), 3.35–3.39 (m, 4H). ^{13}C NMR (101 MHz, DMSO-d_6) δ 153.52, 151.91, 150.72, 148.30, 147.89, 145.18, 145.11, 141.44, 134.58, 132.80, 131.24, 130.28, 127.46, 126.13, 126.01, 123.10, 120.53, 119.71, 118.80, 115.56, 47.26, 47.05, 45.77. HRMS (ESI): calcd for $C_{24}H_{24}N_5O_6S^+$ (M^+) 510.1442, found 510.1443.

2.2. Fluorescence colocalization experiments

MCF-7 cells were co-cultured with Mito-Tracker Green (200 nM) and **MITO-PQDNs** (10 μM) for 60 min, and then subjected to fluorescence imaging. Finally, the co-localization analysis of the imaging results was performed using ImageJ.

3. Results and discussion

3.1. Spectroscopic properties of MITO-PQDNs towards GSH

First, we comprehensively tested the UV-Vis absorption spectra and fluorescence spectra of the probe **MITO-PQDNs** (10 μM) before and after the reaction with GSH (1 mM) in phosphate-buffered saline (PBS, pH 7.4, 10 mM). It can be seen from Fig. 1 that the maximum absorption peak of **MITO-PQDNs** was located at 400 nm, and the emission spectra of **MITO-PQDNs**

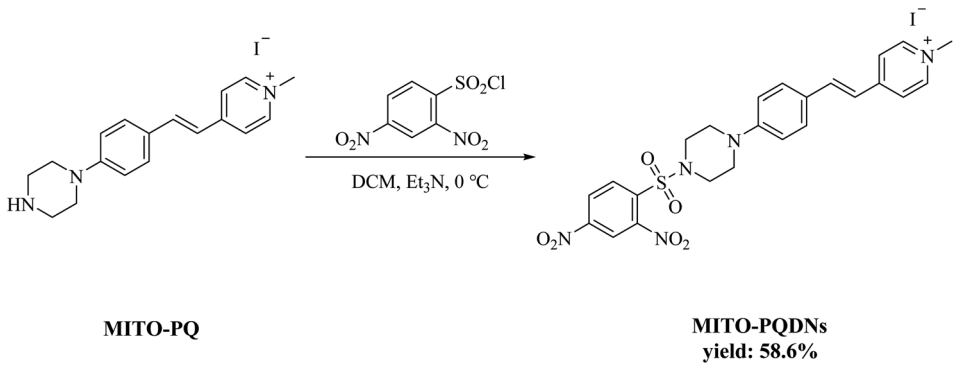

Scheme 2 Synthetic route for the probe MITO-PQDNs.

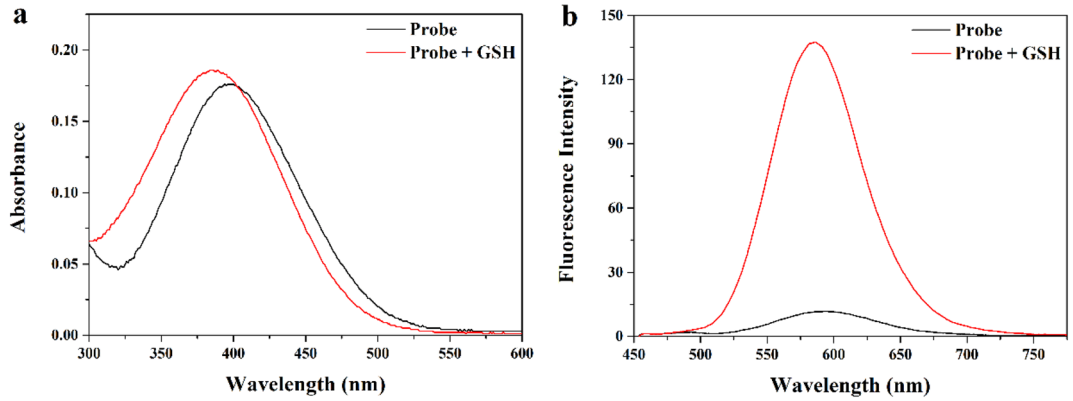

Fig. 1 (a) Absorption and (b) fluorescence responses of **MITO-PQDNs** (10 μM) to GSH (1 mM) in PBS (10 mM, pH 7.4).

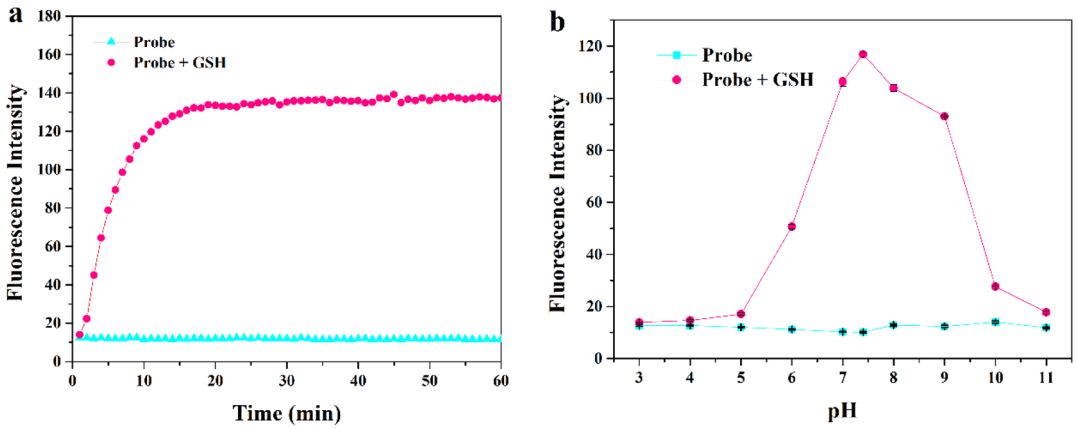

Fig. 2 (a) Time-dependent emission intensity of **MITO-PQDNs** (10 μM) towards GSH (1 mM) at 586 nm. (b) Fluorescence response of **MITO-PQDNs** (10 μM) at different pH values (3–11).

exhibited a weak fluorescence signal at 586 nm. After adding GSH, the maximum absorption peak was blue-shifted from 400 nm to 386 nm, indicating that **MITO-PQDNs** reacted with GSH to form a new substance. During this process, a marked increase in fluorescence intensity (586 nm) and a significant Stokes shift (200 nm) were exhibited. The above spectral data showed that **MITO-PQDNs** could react with GSH, thus achieving a fluorescence "off–on" switch. Meanwhile, the fluorescence intensity at 586 nm reached the maximum when **MITO-PQDNs** reacted with GSH for 20 min (Fig. 2a). When the reaction time was further extended to 60 min, there was no significant change in the fluorescence intensity at 586 nm, while **MITO-PQDNs**

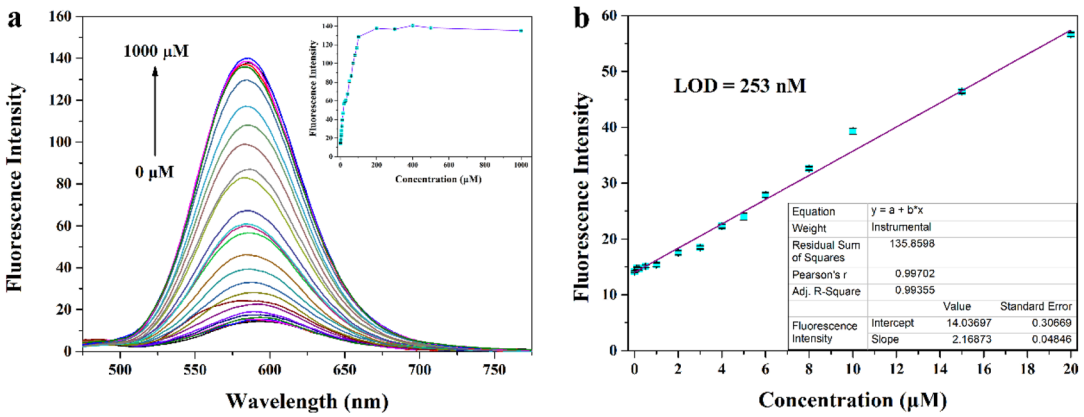

Fig. 3 (a) Fluorescence titration curves of **MITO-PQDNs** (10 μM) for different concentrations of GSH. (b) The linear relationship of fluorescence intensity at 586 nm *versus* the concentrations of GSH (0–20 μM).

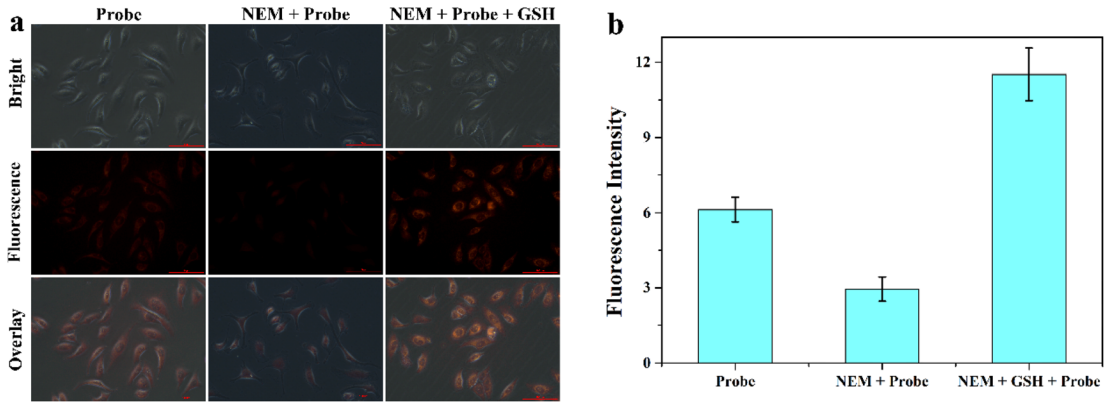

Fig. 4 (a) Fluorescence imaging of GSH in MCF-7 cells using **MITO-PQDNs** (10 μM). (b) The relative fluorescence intensity of MCF-7 cells in different groups. Scale bar: 100 μm.

itself did not emit a strong fluorescence signal from the beginning to the end. The above results demonstrated that **MITO-PQDNs** owned excellent photostability and a fast response rate for GSH in PBS buffer solution.

Subsequently, we studied the fluorescence response of **MITO-PQDNs** to GSH at different pH values. The fluorescence intensity of **MITO-PQDNs** itself did not change with pH, indicating that **MITO-PQDNs** was stable in the pH range of 3–11 (Fig. 2b). After the addition of GSH, a strong fluorescent signal was seen in the pH range of 6–9. These results suggested that **MITO-PQDNs** could detect GSH at physiological and have the potential for bioimaging applications.

3.2. Selectivity and sensitivity

Considering the possible presence of various interferences in the complex biological microenvironment, we think that the selectivity and anti-interference ability of **MITO-PQDNs** towards GSH need to be investigated. We recorded changes in the emission spectra when **MITO-PQDNs** was incubated with 28 kinds of analytes for 20 min. The presence of GSH could trigger a marked increase in fluorescence intensity (586 nm), while the addition of other amino acids (Ala, Glu, Gln, Arg, Val, Asp, Gly, Leu, Ile, His, Tyr, Met, Lys, Phe, Pro, Ser, Thr, Asn, Trp) and ionic compounds ($CaCl_2$, $MgSO_4$, NaF, NaCl, NaBr, KI, NaHS) had almost no effect on the fluorescence spectra (Fig. S4†). However, a slight fluorescence enhancement was displayed after Cys/Hcy were added, which may be due to the nucleophilic properties of Cys and Hcy promoting the breakage of the sulfonamide bond of **MITO-PQDNs**. It was worth mentioning that the concentration of GSH in living cells was approximately 1–10 mM, which was well above that of Cys (30–200 μM) and Hcy (5–15 μM).[29–31] Hence, Cys/Hcy had a negligible effect on

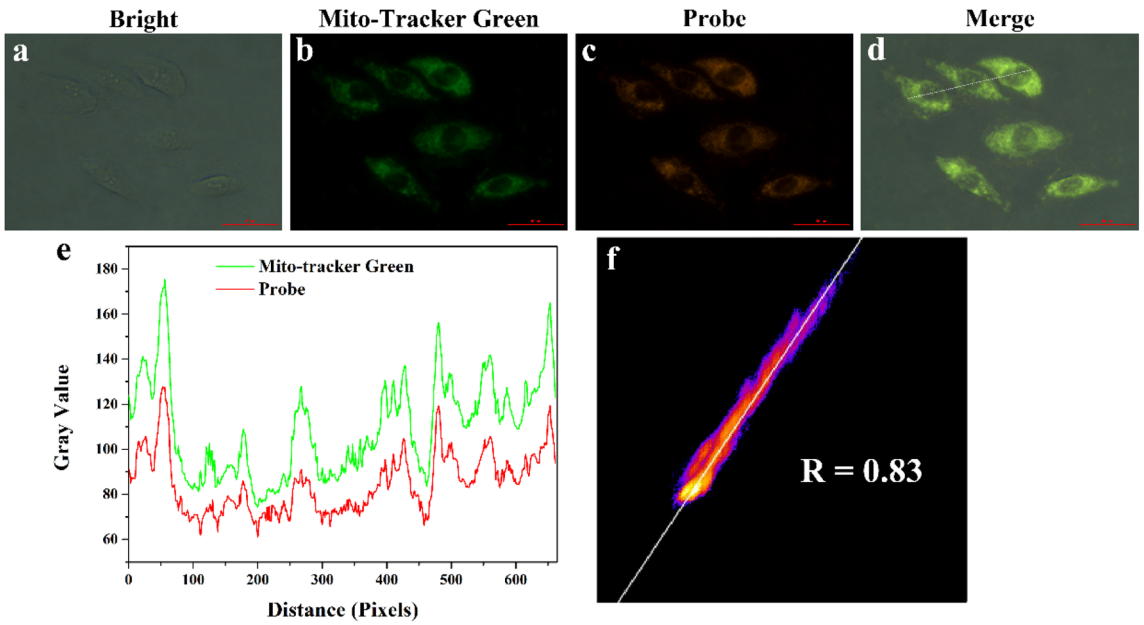

Fig. 5 Subcellular co-localization of **MITO-PQDNs** (10 μM) and Mito-Tracker Green (200 nM) in MCF-7 cells. (a) Bright field image. (b) Green channel. (c) Red channel. (d) Merged image. (e) Fluorescence intensity profiles of the linear region cross MCF-7 cells. (f) Co-localization analysis of **MITO-PQDNs** and Mito-Tracker Green. Scale bar: 50 μm.

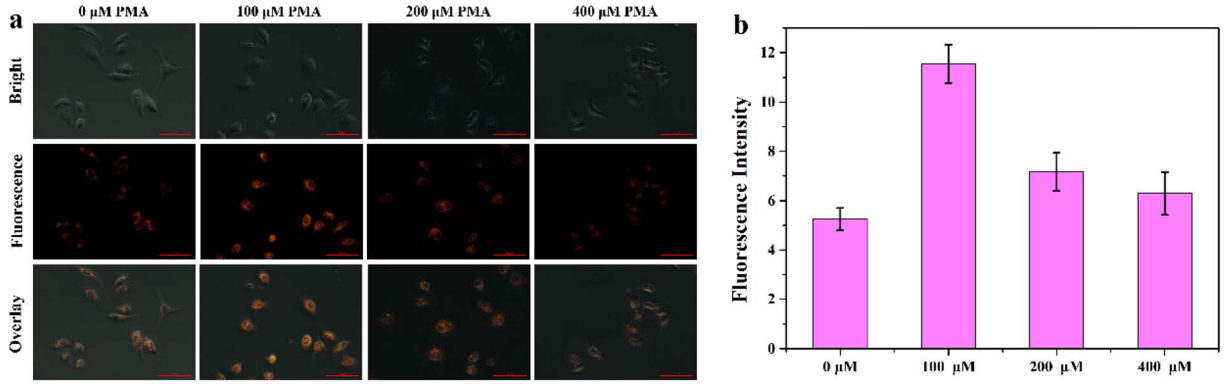

Fig. 6 (a) Fluorescence imaging of GSH in MCF-7 cells pretreated with different concentrations of PMA using **MITO-PQDNs** (10 μM). (b) The relative fluorescence intensity of MCF-7 cells in different groups. Scale bar: 100 μm.

detecting GSH in biological systems. After confirming the selectivity of **MITO-PQDNs** for GSH, the competition experiment was performed (Fig. S4†). The addition of GSH still caused a significant increase in fluorescence intensity at 586 nm when other analytes were present, indicating that **MITO-PQDNs** had a strong anti-interference capacity for the detection of GSH.

To investigate the ability of **MITO-PQDNs** to quantify GSH, we added different concentrations of GSH to the PBS buffer containing **MITO-PQDNs** (10 μM), and the changes in the fluorescence spectra were recorded. The emission intensity at 586 nm gradually enhanced as the GSH concentration increased and basically achieved the maximum value when the GSH concentration was 200 μM (Fig. 3a). From Fig. 3b, the emission intensity (586 nm) was linearly proportional to the GSH concentration in the range of 0–20 μM ($R = 0.99355$), which demonstrated that **MITO-PQDNs** had the potential ability to detect GSH quantitatively. Compared with other reported probes for GSH detection,[32–36] **MITO-PQDNs** had higher sensitivity for GSH with a detection limit as low as 253 nM.

3.3. Response mechanism of MITO-PQDNs towards GSH

According to the published literature, the possible reaction mechanism between **MITO-PQDNs** and GSH was presented in Scheme 1.[20,22,37–39] The strong electron-absorbing DNs group significantly quenched the fluorescence of **MITO-PQDNs**. However, the strongly nucleophilic GSH could undergo a nucleophilic aromatic substitution reaction (SNAr) with **MITO-PQDNs** leading to the cleavage of the sulfonate esters, thus releasing the fluorophore **MITO-PQ**. To better understand the response mechanism, we analyzed the mixture of **MITO-PQDNs** and GSH by HRMS, which verified the formation of **MITO-PQ** (Fig. S5†).

3.4. Cell imaging

Encouraged by the superior properties of **MITO-PQDNs** in PBS buffer, the cellular experiments were carried out in MCF-7 cells to assess its potential biological applications. The cytotoxicity assay was first carried out because biocompatibility was a vital criterion to examine whether the probe could be applied to cellular imaging. The results showed that the cell viability remained approximately 100% upon coincubation with 25 μM probe **MITO-PQDNs** for 12 h (Fig. S6†), which indicated that **MITO-PQDNs** had low cytotoxicity for MCF-7 cells. Subsequently, the capability of **MITO-PQDNs** to detect intracellular GSH was studied in MCF-7 cells. As depicted in Fig. 4, an intense orange fluorescent signal was seen in the MCF-7 cells after 60 min incubation with 10 μM **MITO-PQDNs**. The intracellular fluorescence signal was markedly degraded after pretreatment with 500 μM *N*-ethylmaleimide (NEM, a thiol blocking reagent) for 30 min. However, the bright orange fluorescence was again observed when NEM-pretreated MCF-7 cells were treated with 1 mM GSH for 30 min. The above experimental phenomena demonstrated that the probe **MITO-PQDNs** possessed excellent cell membrane permeability and could detect both endogenous and exogenous GSH in living cells.

To assess the ability of **MITO-PQDNs** to target mitochondria, we performed that MCF-7 cells were co-stained with 200 nM Mito-Tracker Green (a commercial mitochondrial green dye) and 10 μM **MITO-PQDNs** for 60 min. As displayed in Fig. 5, the orange fluorescence emitted from the reaction product of **MITO-PQDNs** and GSH reactant was highly overlapped with the green fluorescence emitted from Mito-Tracker Green, where the Pearson's correlation coefficient was 0.83. The results of the co-localization experiments fully confirmed that the probe could be specifically enriched in mitochondria and enable the visualization of mitochondrial GSH.

After determining the mitochondrial targeting ability of **MITO-PQDNs**, the feasibility of **MITO-PQDNs** in achieving the visual detection of the dynamic changes in mitochondrial GSH concentrations during oxidative stress was investigated. As indicated in Fig. 6, the emission intensity of the MCF-7 cells pretreated with 100 μM phorbol myristate acetate (PMA) was significantly stronger than that of control cells. Nevertheless, the intracellular fluorescence intensity gradually diminished upon increasing the concentration of PMA to 200 and 400 μM. This might be to prevent oxidative damage caused by PMA-induced production of ROS, leading to high expression of GSH. Moreover, the intracellular GSH level would decrease when the excessive production of ROS exceeded the antioxidant

capacity of GSH. These results provided strong evidence that the probe **MITO-PQDNs** could be applied to the visual monitoring of mitochondrial GSH during oxidative stress.

4. Conclusions

All in all, we developed a styrylpyridine derivative-based fluorescent probe **MITO-PQDNs** for monitoring GSH in mitochondria. The probe **MITO-PQDNs** with the DNs recognition group could detect GSH through SNAr in PBS solution and emit a strong fluorescence signal (586 nm) after reaction with GSH. Moreover, **MITO-PQDNs** also had the advantages of significant Stokes shift, superb water solubility, high sensitivity, and low cytotoxicity. Besides, the imaging results strongly demonstrated that **MITO-PQDNs** was able to selectively enrich in mitochondria and visualize mitochondrial GSH fluctuations during oxidative stress. Therefore, the probe **MITO-PQDNs** was a promising chemical sensor for detecting mitochondrial GSH, and its development contributed to studying the antioxidant mechanism of mitochondrial GSH.

Conflicts of interest

There are no conflicts to declare.

References

1 S.-Y. Lim, K.-H. Hong, D. I. Kim, H. Kwon and H.-J. Kim, *J. Am. Chem. Soc.*, 2014, **136**, 7018–7025.
2 D. R. Green, *Cell*, 1998, **94**, 695–698.
3 M. Y. Berezin and S. Achilefu, *Chem. Rev.*, 2010, **110**, 2641–2684.
4 T. Finkel, M. Serrano and M. A. Blasco, *Nature*, 2007, **448**, 767–774.
5 V. Sorrentino, K. J. Menzies and J. Auwerx, *Annu. Rev. Pharmacol. Toxicol.*, 2018, **58**, 353–389.
6 Y.-y. Wang, S.-m. Chen and H. Li, *Acta Pharmacol. Sin.*, 2010, **31**, 160–164.
7 L. Wu, A. C. Sedgwick, X. Sun, S. D. Bull, X.-P. He and T. D. James, *Acc. Chem. Res.*, 2019, **52**, 2582–2597.
8 R. A. J. Smith, R. C. Hartley and M. P. Murphy, *Antioxid. Redox Signaling*, 2011, **15**, 3021–3038.
9 J. C. Fernandez-Checa and N. Kaplowitz, *Toxicol. Appl. Pharmacol.*, 2005, **204**, 263–273.
10 K. Xu and P. J. Thornalley, *Biochem. Pharmacol.*, 2001, **61**, 165–177.
11 Y. Yue, F. Huo, F. Cheng, X. Zhu, T. Mafireyi, R. M. Strongin and C. Yin, *Chem. Soc. Rev.*, 2019, **48**, 4155–4177.
12 M. Vendrell, D. Zhai, J. C. Er and Y.-T. Chang, *Chem. Rev.*, 2012, **112**, 4391–4420.
13 Y. Yang, Q. Zhao, W. Feng and F. Li, *Chem. Rev.*, 2013, **113**, 192–270.
14 X.-L. Liu, L.-Y. Niu, Y.-Z. Chen, M.-L. Zheng, Y. Yang and Q.-Z. Yang, *Org. Biomol. Chem.*, 2017, **15**, 1072–1075.
15 W. Shu, J. Yu, H. Wang, A. Yu, L. Xiao, Z. Li, H. Zhang, Y. Zhang and Y. Wu, *Anal. Chim. Acta*, 2022, **1220**, 340081.
16 Z. Xu, X. Huang, X. Han, D. Wu, B. Zhang, Y. Tan, M. Cao, S. H. Liu, J. Yin and J. Yoon, *Chem*, 2018, **4**, 1609–1628.
17 Y.-L. Zheng, Z.-H. Chai, W. Tang, S. Yan, F. Dai and B. Zhou, *Sens. Actuators, B*, 2021, **330**, 129343.
18 S. Qi, W. Liu, P. Zhang, J. Wu, H. Zhang, H. Ren, J. Ge and P. Wang, *Sens. Actuators, B*, 2018, **270**, 459–465.
19 T. Jin, M. Cui, D. Wu, W. Zhu, Y. Xu and X. Qian, *Chin. Chem. Lett.*, 2021, **32**, 3899–3902.
20 M. Jia, L. Wei, Y. Lu, R. Zhang, Q. Chen, W. Xia, Y. Liu, F. Li and Y. Zhou, *RSC Adv.*, 2022, **12**, 2668–2674.
21 B. Ma, D.-H. Tian, S. Yan, X.-C. Li, F. Dai and B. Zhou, *Sens. Actuators, B*, 2021, **327**, 128937.
22 J. Chen, Z. Wang, M. She, M. Liu, Z. Zhao, X. Chen, P. Liu, S. Zhang and J. Li, *ACS Appl. Mater. Interfaces*, 2019, **11**, 32605–32612.
23 X. Zhong, Q. Yang, Y. Chen, Y. Jiang, B. Wang and J. Shen, *J. Mater. Chem. B*, 2019, **7**, 7332–7337.
24 C. Wang, Y. Wang, G. Wang, C. Huang and N. Jia, *Anal. Chim. Acta*, 2020, **1097**, 230–237.
25 X.-B. Wang, H.-J. Li, C. Liu, W.-Y. Lu, X. Lu and Y.-C. Wu, *Dyes Pigm.*, 2022, **199**, 110058.
26 X. Lu, Z. Chen, X. Dong and W. Zhao, *ACS Sens.*, 2018, **3**, 59–64.
27 J. Xu, C. Wang, Q. Ma, H. Zhang, M. Tian, J. Sun, B. Wang and Y. Chen, *ACS Omega*, 2021, **6**, 14399–14409.
28 L. Fan, Q. Zan, X. Wang, X. Yu, S. Wang, Y. Zhang, Q. Yang, W. Lu, S. Shuang and C. Dong, *Chem. Eng. J.*, 2022, **449**, 137762.
29 H. Zhang and Z. Fang, *RSC Adv.*, 2018, **8**, 11419–11423.
30 H. Ren, F. Huo and C. Yin, *New J. Chem.*, 2021, **45**, 9096–9101.
31 Y. Z. Yang, Z. Y. Xu, L. Han, Y. Z. Fan, M. Qing, N. B. Li and H. Q. Luo, *Dyes Pigm.*, 2021, **184**, 108722.
32 P. Su, Z. Zhu, Y. Tian, L. Liang, W. Wu, J. Cao, B. Cheng, W. Liu and Y. Tang, *Talanta*, 2020, **218**, 121127.
33 Y. Mao, Y. Xu, Z. Li, Y. Wang, H. Du, L. Liu, R. Ding and G. Liu, *Sensors*, 2019, **19**, 5348.
34 H. Zhou, J. Tang, L. Lv, N. Sun, J. Zhang, B. Chen, J. Mao, W. Zhang, J. Zhang and J. Zhou, *Analyst*, 2018, **143**, 2390–2396.
35 Y. Wan, Y. Li, Z. Liao, Z. Tang, Y. Li, Y. Zhao and B. Xiong, *Spectrochim. Acta, Part A*, 2019, **223**, 117265.
36 Y.-L. Fu, X.-G. Chen, H. Li, W. Feng and Q.-H. Song, *New J. Chem.*, 2020, **44**, 13781–13787.
37 L. Fan, W. Zhang, X. Wang, W. Dong, Y. Tong, C. Dong and S. Shuang, *Analyst*, 2019, **144**, 439–447.
38 R. Li, X. Huang, G. Lu and C. Feng, *RSC Adv.*, 2018, **8**, 24346–24354.
39 J. Wang, H. Wang, Y. Hao, S. Yang, H. Tian, B. Sun and Y. Liu, *Food Chem.*, 2018, **262**, 67–71.